Respiratory Research

RESEARCH

Open Access

A novel technique of cryodenervation for murine vagus nerve: implications for acute lung inflammation

Di Wu[1†], Ximing Liao[1†], Jing Gao[1†], Kun Wang[1], Wujian Xu[1], Feilong Wang[1], Zhixian Jin[2], Dandan Wu[3*], Qiang Li[1*] and Wei Gao[1*]

Abstract

Background Neuroimmune interaction is an underestimated mechanism for lung diseases, and cryoablation is a competitive advantageous technique than other non-pharmacologic interventions for peripheral nerve innervating the lung. However, a lack of cryodenervation model in laboratory rodents leads to the obscure mechanisms for techniques used in clinic.

Method Herein, we developed a novel practical method for mouse peripheral nerve cryoablation, named visualized and simple cryodenervation (VSCD). We first estimated the feasibility, safety and effectiveness of the technique via haematoxylin-eosin staining, histochemistry or immunofluorescence staining and immunoblotting assay. We then constructed the acute lung injury (ALI) model triggered by lipopolysaccharide (LPS) to verify the effect of VSCD in the resolution of pulmonary inflammation. Besides, the *IL-10* knockout mice were also applied to explain the underlying mechanism of the protective activity of VSCD in ALI mice.

Result We demonstrated that VSCD was able to induce a reliable and stable blockade of innervation, but reversible structural damage of mouse vagus nerve without detectable toxicity to lung tissues. Cholinergic parasympathetic nerve in the mouse lung coming from vagus nerve was activated at the initial stage (1 week) after VSCD, and blocked 3 weeks later. By use of the ALI mouse model, we found that VSCD effectively decreased pulmonary inflammation and tissue damage in the ALI mice. Moreover, the activated cholinergic anti-inflammatory pathway (CAP) and elevated IL-10 expression might explain the protective action of VSCD following LPS challenge.

Conclusion This study fills the gap in the cryoablation for mouse vagus nerve, thereby guiding the application of cryodenervation in clinical management of pulmonary diseases. It also offers evidence of anti-inflammatory potential of VSCD in ALI mouse model and opens therapeutic avenues for the intervention of acute lung inflammation.

[†]Di Wu, Ximing Liao and Jing Gao contributed equally to this work.

*Correspondence:
Dandan Wu
wuedandan@126.com
Qiang Li
liqressh1962@163.com
Wei Gao
grace19881118@126.com

Full list of author information is available at the end of the article

Keywords Cryodenervation, Vagus nerve, Lung innervation, Acute lung injury, Interleukin-10

Background

Cryoablation is a technique referring to the application of freezing temperatures (below − 75 °C) to destroy targeted tissues and also known as cryosurgery, cryotherapy or percutaneous cryoablation. Cryoablation was first applied into clinical practice in the middle of 19th century for the treatment of uterine and breast cancer. Since then, the development of low-temperature physics and engineering, as well as the invention of sophisticated instruments using cryogens like liquid nitrogen and high-pressured argon gas led to the widespread clinical usage of this technique [1]. In addition to directly eliminating solid tumor lesions [2], cryoablation is able to stimulate the release of tumor antigens, activate immune responses and amplify the effect of immunotherapy [3], which play an increasingly important role in anti-tumor therapeutic options. Besides, percutaneous cryoablation has also proven beneficial in alleviating metastatic chest or pleuritic pain, and refractory chronic peripheral neuropathy pain [4, 5]. When it comes to initial treatment of atrial fibrillation, cryoablation shows lower recurrence rate, less symptomatic atrial tachyarrhythmia and serious adverse event than conventional antiarrhythmic drugs [6].

With respect to lung diseases, cryoablation causes less damage to low water-content tissue like bronchial wall than radiofrequency or microwave [7]. In the management of non-small cell lung cancer, a series of clinical trials combining immune check point inhibitors and percutaneous cryoablation have been in progress to evaluate the efficacy and safety of cryo-immunotherapy [8]. Considering the cholinergic hyperactivity and neurogenic over-inflammation in chronic airway diseases, targeted lung denervation (TLD) towards both vagal afferent and parasympathetic efferent fibers may become a predominant therapeutic technique for chronic obstructive pulmonary disease (COPD). TLD by bronchoscopic radiofrequency could alleviate bronchoconstriction and mucous hyper-secretion, thus reducing acute exacerbations and adverse events in COPD patients [9, 10]. To further optimize the safety and wound healing, our group has developed a novel cryo-balloon TLD system called bronchial cryodenervation (BCD) [11], which was found to effectively ameliorate the symptoms of the patients with severe asthma [12].

Due to the critical role of cryodenervation in clinical practice, the demand for relevant animal models in basic scientific research has greatly increased. For large laboratory animals like canine and sheep, an adoption of clinic TLD instruments is feasible; for example, the BCD system developed by our group was applied for pulmonary denervation of sheep [11]. However, when it comes to small laboratory rodents widely used in scientific research, there is still a lack of simple and effective cryodenervation model. The current methods for vagus nerve blocking in rodents only include vagotomy and neuroanesthesia: the former can lead to a permanent and irreversible damage, while the latter causes reversible but temporary blockage [13], which are both inconsistent with clinical requirements and leave a gap for long-term and reversible nerve blockage. Notably, nerve perineurium and epineurium keep integrated after cryoablation, serving as a conduit for axon self-repair varying from several hours to months depending on freezing temperature and time [14].

Herein, we developed a practical method for mouse peripheral nerve cryoablation using common laboratory equipments, which is named visualized and simple cryodenervation (VSCD). Specifically, a liquid nitrogen-cooled pen (-196℃) is applied to freeze right cervical vagus nerve under stereomicroscope, thereby disrupting the structure and function of sensory and parasympathetic fibers innervating the lung (Fig. 1, Movie S1). In this study, we first estimated the feasibility, safety and effectiveness of VSCD procedure. Morphological damage of the nerve was assessed via histochemistry staining, while the innervation changes were evaluated by the detection of neural marker and neurotransmitter in the lung. Due to the transient hyperactivity of cholinergic fibers, VSCD was then used in a mouse model of acute lung injury (ALI) and found to exert a protective role in relieving pulmonary inflammatory damage. Mechanistically, VSCD could activate the cholinergic anti-inflammatory pathway (CAP) and upregulate endogenous interleukin-10 (IL-10) expression, thus offering novel therapeutic option for the intervention of acute lung inflammation like ALI.

Methods

Study approval

All experiments performed on animals were in accordance with the guide for Care and Use of Laboratory Animals from Shanghai Committee. Meanwhile, the research protocol has been recognized by Laboratory Animal Research Center Review Board of Tongji University (Permit Number: TJBB03721106) (Shanghai, China). All operations were conducted under pentobarbital sodium anesthesia, and every effort was made to minimize animal suffering and the number of animals used.

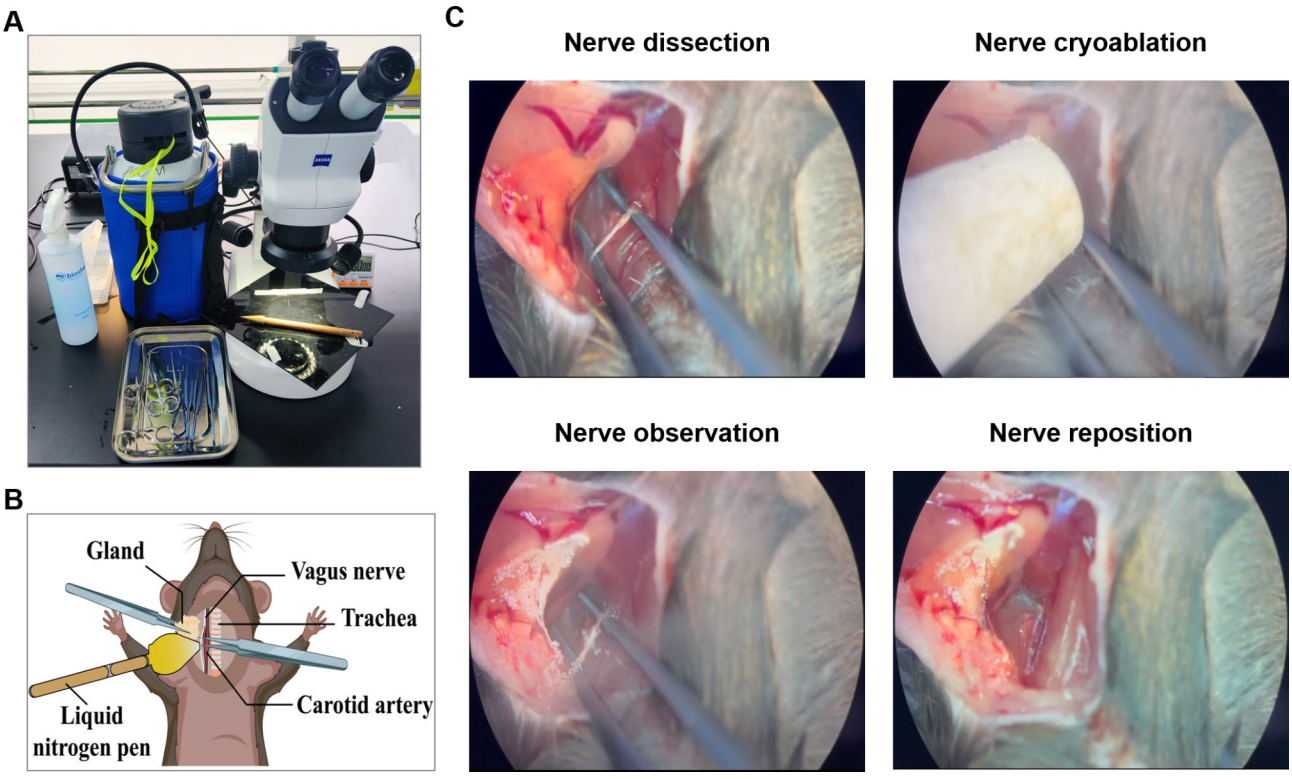

Fig. 1 The novel practical method for mouse vagus nerve cryoablation. **(A)** The instruments required for VSCD mainly include liquid nitrogen tank, liquid nitrogen pen, stereomicroscope, microforceps, 75% alcohol, operating board, ophthalmic curved scissors, hemostat, forceps, and timer. **(B)** Experimental strategy for VSCD. **(C)** Mouse right cervical vagus nerve was bluntly separated from adjacent carotid artery by forceps. Then, the pre-cooled liquid nitrogen pen was used to freeze the nerve for 5/10/15s, with the attention should be paid to avoiding compressing surrounding tissues. After removing the pen, frost formation on the nerve was observed in a short time and indicated a successful cryoablation, followed by rapidly disappearing of the frost, which suggested the rewarming process of the nerve

Unilateral VSCD procedure

Eighty mice were randomly divided into 16 groups (5 mice/group): Sham group, VSCD-5s group, VSCD-10s group, and VSCD-15s group at 1, 2, 3, and 4 weeks post-operation, respectively (Figs. 2, 3 and 4). Use a lifting tube to transfer liquid nitrogen from the large liquid nitrogen tank to a small liquid nitrogen container, and place the liquid nitrogen pen in the container for cooling and standby. Anesthetize the mouse by intraperitoneal injection of 50 mg/kg, 0.3% sodium pentobarbital, place it in the supine position on the operating board, and fully extend the neck. Shave the hair in the neck area with a sterile shaver, disinfect the surgical site thoroughly with an alcohol swab, and place the mouse's neck region under a stereomicroscope. Make a 1 cm longitudinal incision along the midline of the neck using 100 mm ophthalmic curved scissors, separate the submandibular glands to both sides with microforceps, and use a hemostat to clamp and stretch the right submandibular gland to expose the blood vessels and nerves on the right side of the trachea. Use microforceps to bluntly separate the fascia until the right carotid artery and the parallel vagus nerve are fully exposed. Separate the nerve with microforceps and allow the tips of the forceps to naturally open, with the nerve passing naturally above the forceps tips. With the other hand, take out the liquid nitrogen pen, remove any attached liquid nitrogen, and place the pen on the nerve within the forceps. After the intervention time, remove the liquid nitrogen pen and allow the nerve to naturally rewarm. Remove the microforceps, reposition the submandibular glands, suture the wound with absorbable sutures, disinfect thoroughly, and apply a suitable amount of antibiotic ointment locally (Fig. 1, Movie S1).

Histological, immunohistochemical, and immunofluorescence analysis of the vagus nerve and lung tissue

At different time points within 4 weeks after VSCD or sham surgery, right cervical vagus nerves were harvested and fixed in 10% neutral formaldehyde. The samples were then embedded in paraffin, cut into 4-μm sections and flattened on a glass slide, followed by haematoxylin-eosin (H&E) staining. The extent of neuronal injury was evaluated by quantifying the ratio of vacuolated area to total cross-sectional area of the vagus nerve with ImageJ

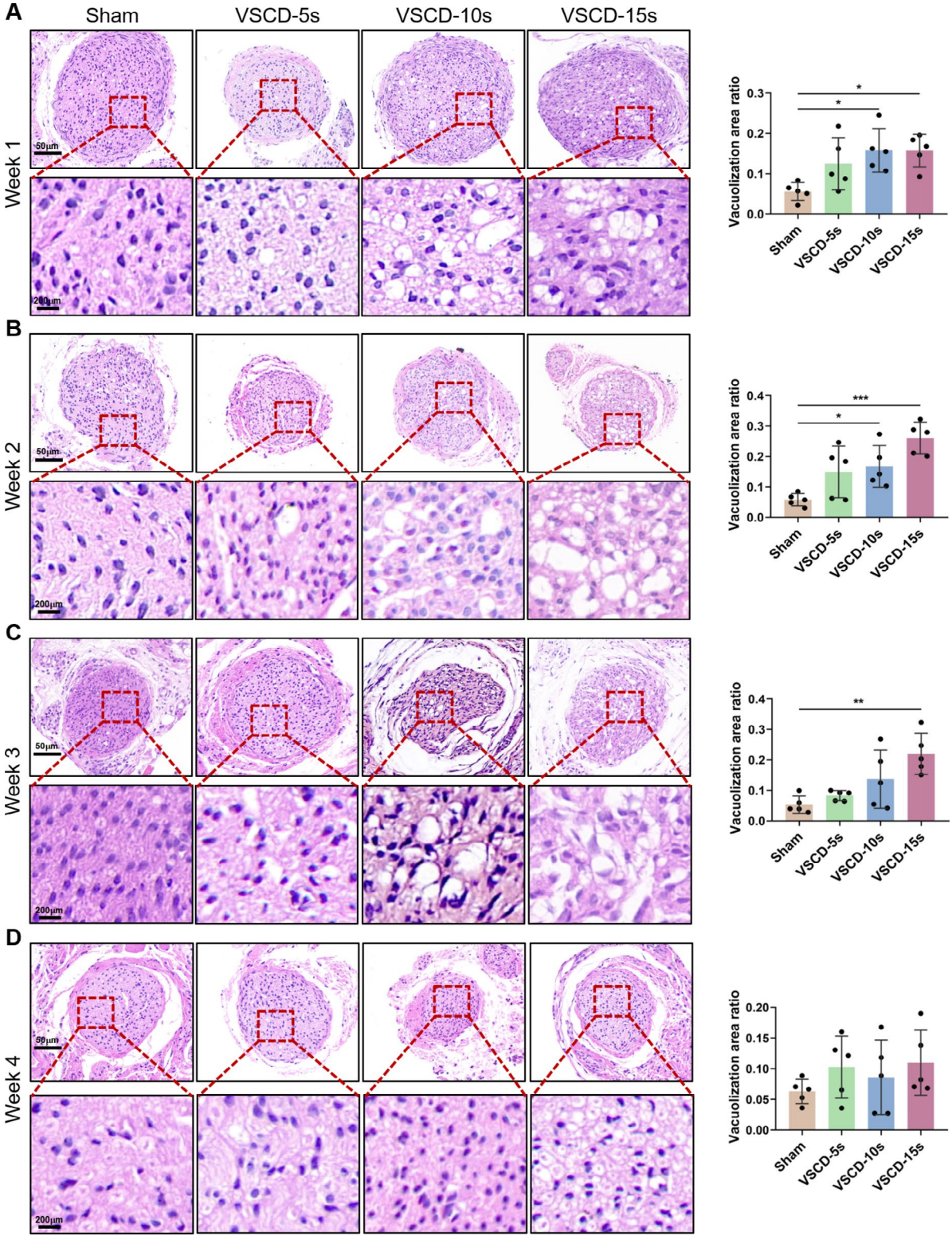

Fig. 2 Histopathological evaluation of VSCD. **(A-D)** The effacement of the nerve architecture and vacuolar degeneration could be observed clearly in the neuronal tissue at week 1 and week 2 **(A, B)**, while recovered after 3 weeks **(C, D)** after VSCD. Scale bar: 50 μm in the upper panel, 200 μm in the below panel. The extent of neuronal injury was evaluated by quantifying the ratio of vacuolated area to total cross-sectional area of the vagus nerve. $n = 5$ per group. *$p < 0.05$, **$p < 0.01$, ***$p < 0.001$. Error bars represented mean ± SEM. Statistical analysis was performed using one-way ANOVA followed by Bonferroni's post hoc test

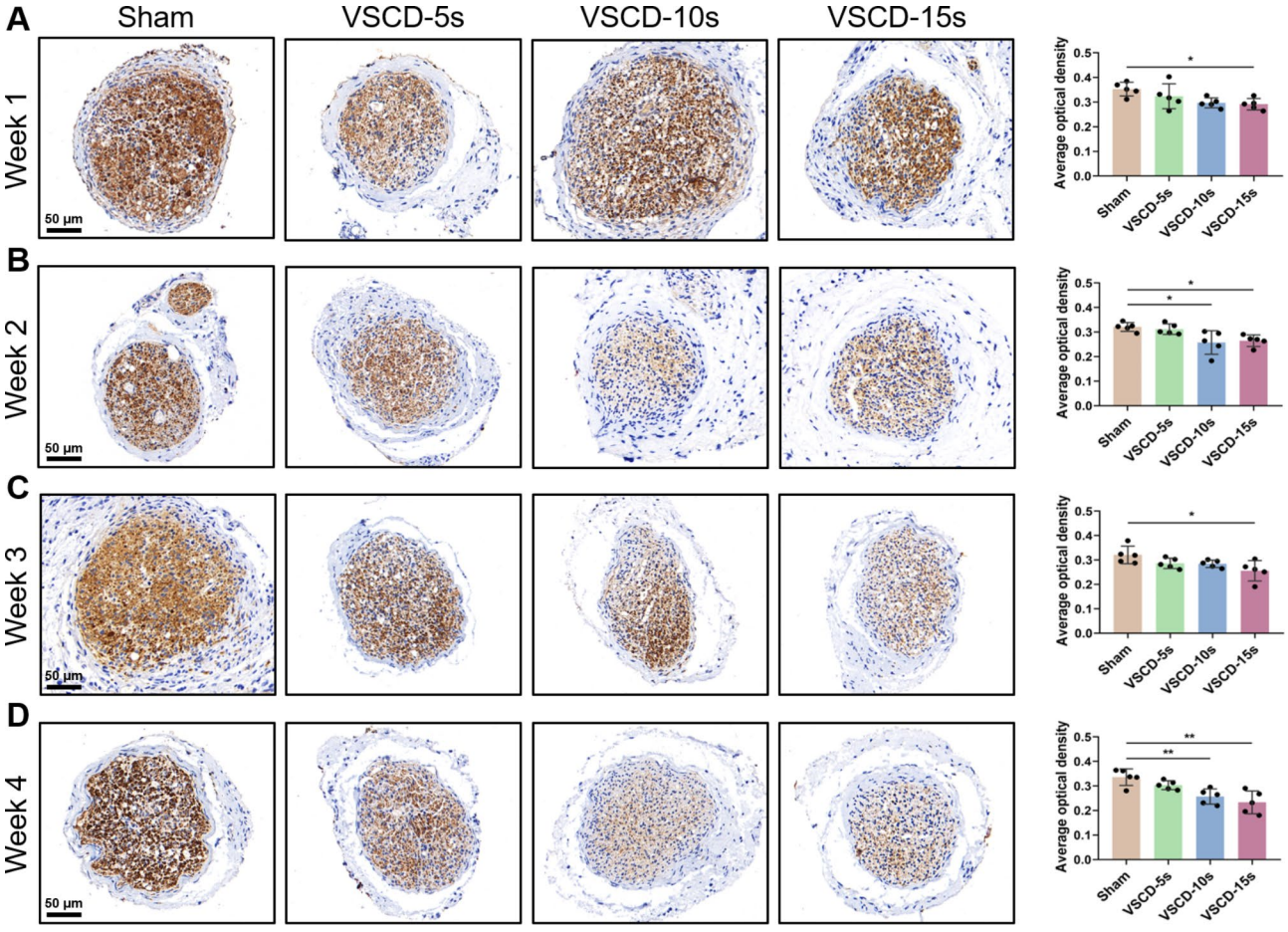

Fig. 3 Immunohistochemical examination of VSCD. **(A-D)** Immunohistochemical staining and the quantitative analysis of pan-neuronal marker PGP9.5 in the nerve samples with or without VSCD procedure. After 2 weeks post VSCD, a significant decrease in PGP9.5 expression indicated a disruption of vagal innervation by the operation. Scale bar: 50 μm. $n = 5$ per group. $^{*}p < 0.05$, $^{**}p < 0.01$. Error bars represented mean ± SEM. Statistical analysis was performed using one-way ANOVA followed by Bonferroni's post hoc test

software (version 1.44p, National Institutes of Health, USA) according to previous literature [15]. The above slides were also immune-stained with the well-established neuronal marker anti-PGP9.5 (Servicebio, China) to quantify alterations in vagus nerve plasticity. Images were acquired via a Nikon Eclipse C1 microscope (Nikon, Japan) and the average optical density of PGP9.5 was determined using ImageJ software in a blinded fashion.

Meanwhile, ipsilateral lung tissues were preserved in 10% neutral formaldehyde, embedded with paraffin, and sliced into sections. The sections were then stained with H&E and imaged under the microscope (Nikon, Japan). The slides were also immune-stained with anti-TRPA1 (Proteintech, USA), anti-ChAT (Servicebio, China), and anti-TH (Servicebio, China) antibodies to determine the impact of VSCD on pulmonary innervation. Images were acquired on the Nikon Eclipse C1 microscope.

LPS-challenged ALI mouse model

The B6.129P2-*Il10*$^{tm1/Nju}$ (*IL-10*$^{-/-}$) mice and C57BL/6 mice (7–8 weeks old, male) were obtained from Shanghai Model Organisms Center, Inc. (Shanghai, China) and kept under specific pathogen-free conditions with a standard 12 h light-dark cycle and unrestricted food/water supply. Forty C57BL/6 mice were randomly divided into 4 groups (10 mice/group): Sham-control group, VSCD-control group, Sham-LPS group, and VSCD-LPS group (Figs. 5 and 6). While *IL-10*$^{-/-}$ mice could be randomly divided into 2 groups (8 mice/group): Sham-LPS group and VSCD-LPS group (Fig. 7). Among them, half is used for bronchoalveolar lavage, and the other is subjected to pathological section of lung tissues. Specifically, after one week of VSCD or sham operation, LPS (10 mg/kg, Sigma-Aldrich, L2630, USA) or PBS were intranasally administered to the mice, which were then sacrificed 24 h later for evaluation of lung inflammation and injury.

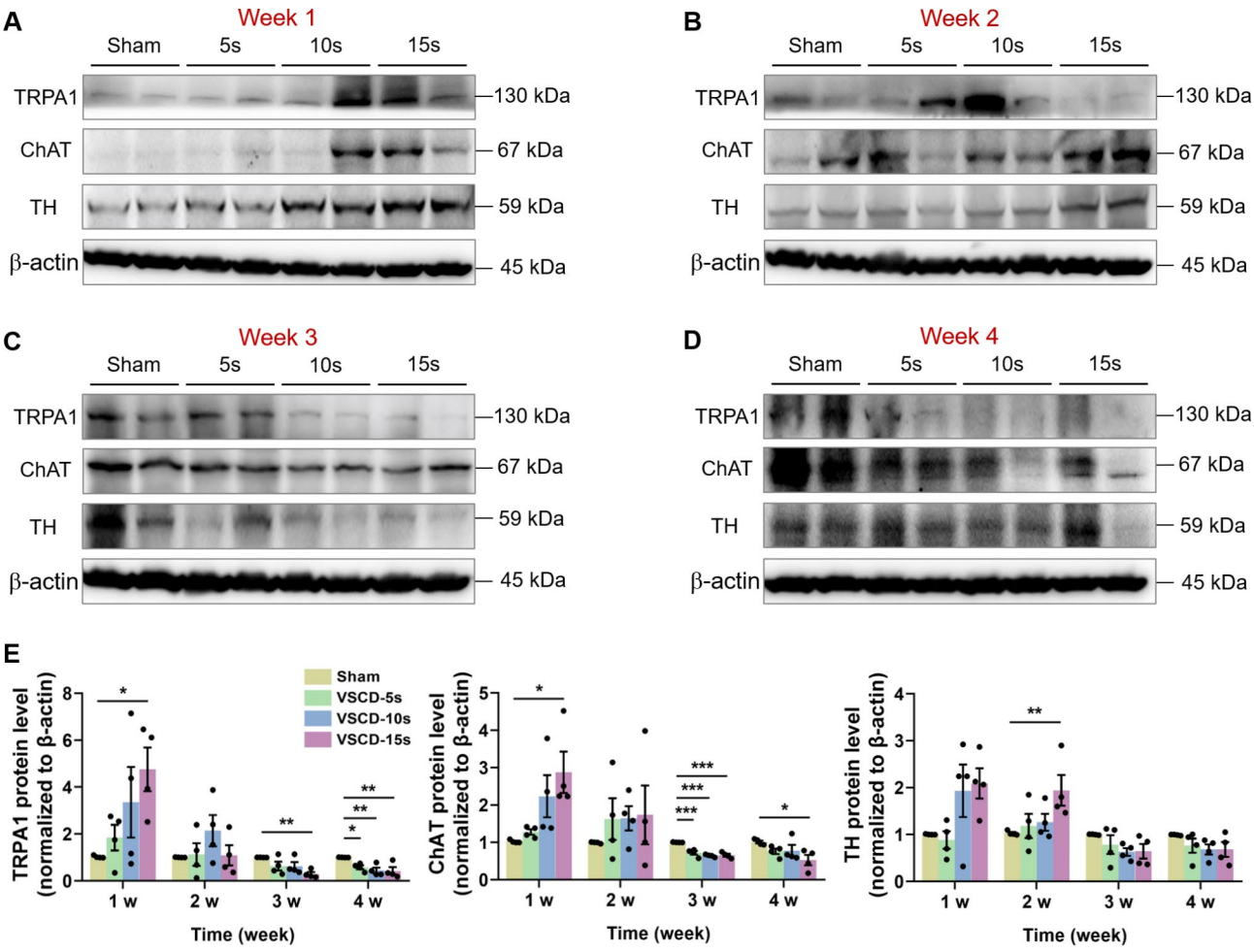

Fig. 4 VSCD alters vagal innervation of the mouse lung. **(A-E)** WB assay **(A-D)** and the quantitative analysis **(E)** exhibiting the effects of VSCD procedure on TRPA1 for sensory nerve activation, ChAT for parasympathetic nerve innervation, and TH for sympathetic nerve activation. $n = 4$ per group. $^{*}p < 0.05$, $^{**}p < 0.01$, $^{***}p < 0.001$. Error bars represented mean ± SEM. Statistical analysis was performed using two-way ANOVA followed by Bonferroni's post hoc test

Bronchoalveolar lavage fluid (BALF) collection and detection

After anesthetization, 0.8 mL ice-cold sterile PBS was slowly infused into the lung through trachea and carefully withdraw. The recovery for the injected volume was basically consistent within each mouse (> 70%), which was called bronchoalveolar lavage fluid. BALF samples were then centrifuged at 4 ℃, 140 × g for 10 min to separate cells and supernatant. On one hand, the precipitated cells were resuspended with 1 mL PBS, followed by total number counting with the automated cell counter (Countess II, Thermo Fisher Scientifc Inc, USA). Afterwards, the cells were fixed onto a glass slide using a cytospin (StatSpin, USA) at 1000 rpm for 4 min, and stained with Wright-Giemsa (Baso Diagnostics, China) for differential leukocyte counts under a microscope in a blinded fashion for at least 200 cells per slide. On the other hand, the supernatant of BALF was used to detect chemokine/cytokine keratinocyte-derived chemokine (KC), IL-6, and neurotransmitter acetylcholine (Ach) by means of ELISA kits (MultiSciences Biotech, China; Abcam, UK) following the manufacturer's protocols.

Serum acquisition and measurement

Blood was obtained by cardiac puncture with a syringe and moved to an Eppendorf Micro Test tube. After standing for more than 1 h at room temperature, the serum sample was collected after centrifuging at 2380 × g for 10 min. The production of cytokines and neurotransmitter in serum of each mouse was quantified via ELISA kits. The measured cytokines include KC (MultiSciences Biotech, China), IL-6 (MultiSciences Biotech, China), and Ach (Abcam, UK).

Histopathological and immunofluorescence assessment of lung tissues

In a separate experiment without BAL, the right lungs were removed and preserved in 10% neutral

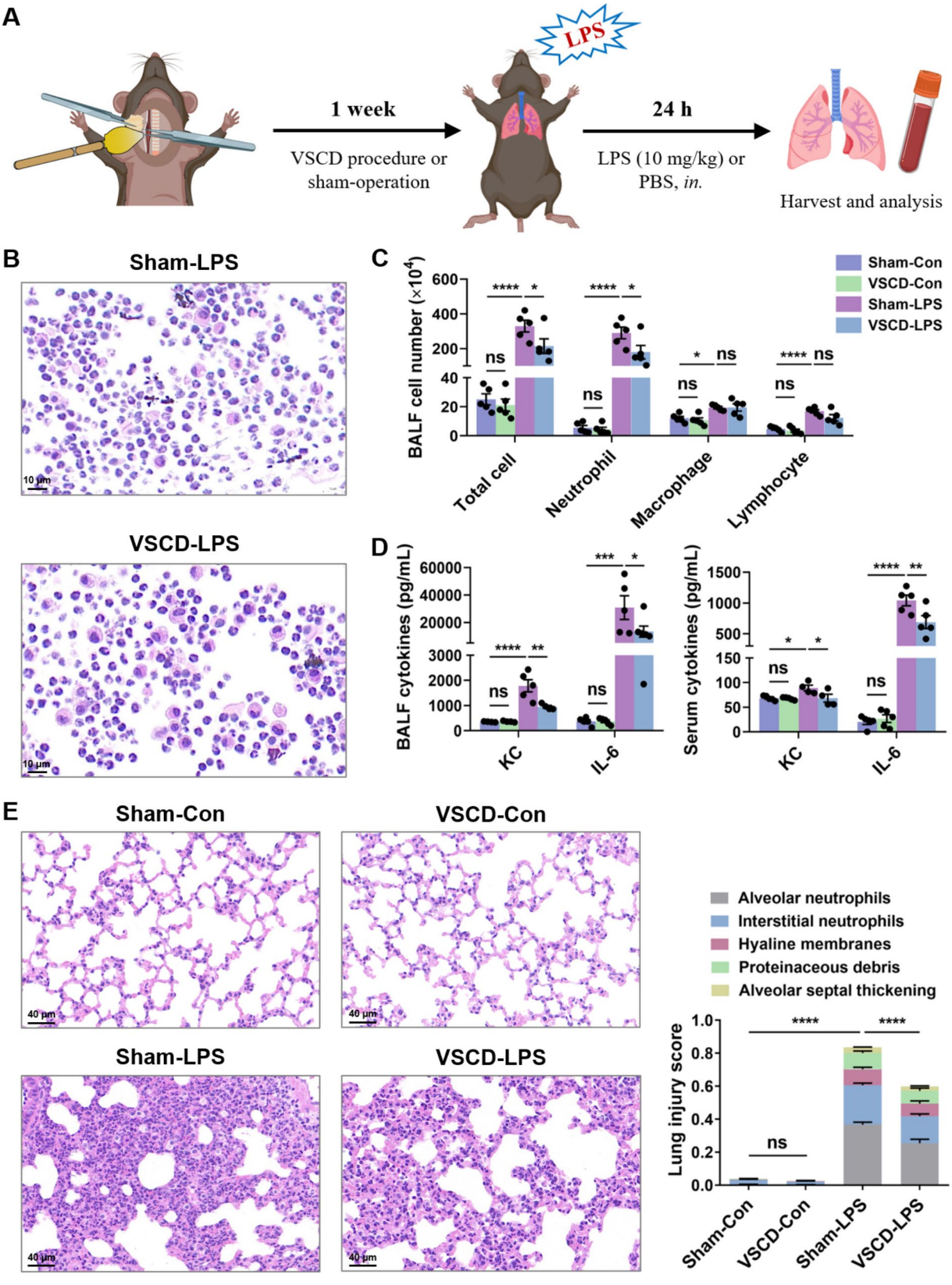

Fig. 5 (See legend on next page.)

(See figure on previous page.)

Fig. 5 VSCD (15s) prevents acute inflammation and tissue damage in the lungs of ALI mice. **(A)** Experimental strategy for the effectiveness evaluation of VSCD in a classical ALI mouse model. C57BL/6 mice were subjected to 15s-VSCD or sham-operation randomly, followed by instillation with 10 mg/kg LPS or PBS intranasally 1 week later. After 24 h, mice were euthanized and BALF, serum and lung tissue were collected for detection. **(B, C)** VSCD (15s) inhibited the aggregation of total leukocytes, especially neutrophils in the BALF of ALI mice. Scale bar: 10 μm. **(D)** VSCD (15s) suppressed the secretion of pro-inflammatory cytokines KC and IL-6 in BALF and serum of ALI mice. **(E)** Representative histological images of lung sections stained with H&E from each group. Scale bar: 40 μm. The injury score was calculated based on the five pathophysiological features. $n = 4–5$ per group. $^{*}p < 0.05$, $^{**}p < 0.01$, $^{***}p < 0.001$, $^{****}p < 0.0001$, ns: not significant. Error bars represented mean ± SEM. Statistical analysis was performed using one-way ANOVA followed by Bonferroni's post hoc test

formaldehyde, followed by embedding, slicing and H&E staining. The slides were imaged under microscope, which were blindly evaluated by pathologist for severity of lung damage via a reliable scoring system [16]. Specifically, total injury score of each sample was calculated from six randomly chosen fields based on five histological variables: neutrophils within alveolar space, neutrophils in interstitial space, hyaline membranes, proteinaceous debris filling airspaces, as well as alveolar septal thickening. Each variable was scored as 0, 1, or 2 in line with the severity, along with different weighting according to the relevance to ALI. The sum of the variables was then normalized to the number of fields, yielding a continuous value between 0 and 1.

Besides, the slides were immune-stained with anti-ChAT (Servicebio, China) and anti-IL-10 (Abcam, UK) antibodies to explore the mechanism underlying the protective effect of VSCD on acute lung inflammation. Images were obtained on the Nikon Eclipse C1 microscope. The integrated density in each slice was determined using ImageJ software in a blinded fashion.

Western blotting (WB) assay

By use of WB assay, the protein levels of transient receptor potential ankyrin 1 (TRPA1), choline acetyltransferase (ChAT), tyrosine hydroxylase (TH) for different nerve systems, NLRP3, Caspase-1 for inflammatory activation, and IL-10, HO-1 for anti-inflammatory activity were measured. Briefly, total proteins were extracted from lung tissues by RIPA buffer (Beyotime, China) and quantified via BCA protein assay kit (Beyotime, China). Equal amounts of protein samples were resolved on 10% SDS PAGE and transferred to a PVDF membrane (Millipore, USA). Nonspecific sites were blocked with Tris-buffered saline containing 0.1% Tween 20 (TBST) and 5% non-fat milk for 2 h at room temperature. The blots were then incubated with primary antibodies against TRPA1 (Proteintech, USA), ChAT (Merck, Germany), TH (Zenbio, China), Caspase-1, IL-10 (Abcam, UK), NLRP3, HO-1, β-actin (Cell Signaling Technology, USA) overnight at 4 °C. The next day, strips were rinsed by TBST and incubated with HRP-conjugated secondary IgG antibodies (Cell Signaling Technology, USA) for 1.5 h at room temperature. After washing with TBST again for 3 times, WB images were captured on a Tanon 5200 Multi automatic chemiluminescence image analysis system (Tanon Biotechnology, China), followed by analyzing via the ImageJ software.

Statistical analysis

All the data were displayed as mean ± standard error (SEM) from at least three independent experiments. Meanwhile, the data were analyzed via two-tailed unpaired Student t test, one-way or two-way ANOVA followed by Bonferroni's post hoc test using GraphPad Prism software (version 8.0.1, GraphPad Software, Inc., CA). Normal distribution of the data was validated with Shapiro-Wilk test. Besides, p value less than 0.05 was defined statistically significant.

Results

VSCD is a feasible and safe procedure for mouse vagal denervation

Instead of expensive and giant cryoablation equipment used in clinic, the instruments required for VSCD are commonly available in general laboratories, mainly including liquid nitrogen tank, liquid nitrogen pen, stereomicroscope, microforceps, 75% alcohol, operating board, ophthalmic curved scissors, hemostat, forceps, and timer (Fig. 1A). Notably, the natural rewarming curve of pre-cooled liquid nitrogen pen at ambient temperature (Figure S1) and the significant mass difference between the pen and mouse vagus nerve ensured that the operative temperature could be maintained below − 160 °C during the VSCD. As shown in Fig. 1B and C, right cervical vagus nerve was bluntly separated from adjacent carotid artery by forceps; at this time, hands should be steady to prevent tearing of the nerve nor significant bleeding from nearby major blood vessels. Then, the pre-cooled liquid nitrogen pen was used to freeze the nerve for different times (5, 10, and 15s), with the attention should be paid to avoiding compressing surrounding tissues if at all possible. Although the contact between liquid nitrogen and adjacent tissues had no impact on the survival of mice, the freezing or compression of blood vessels in surrounding tissues might pose a risk of thrombosis. After removing the pen, frost formation on the nerve was observed in a short time and indicated a successful cryoablation, followed by rapidly disappearing of the frost, which suggested the rewarming process of the nerve (Movie S1). During the entire VSCD process, minor bleeding is acceptable and will not affect the

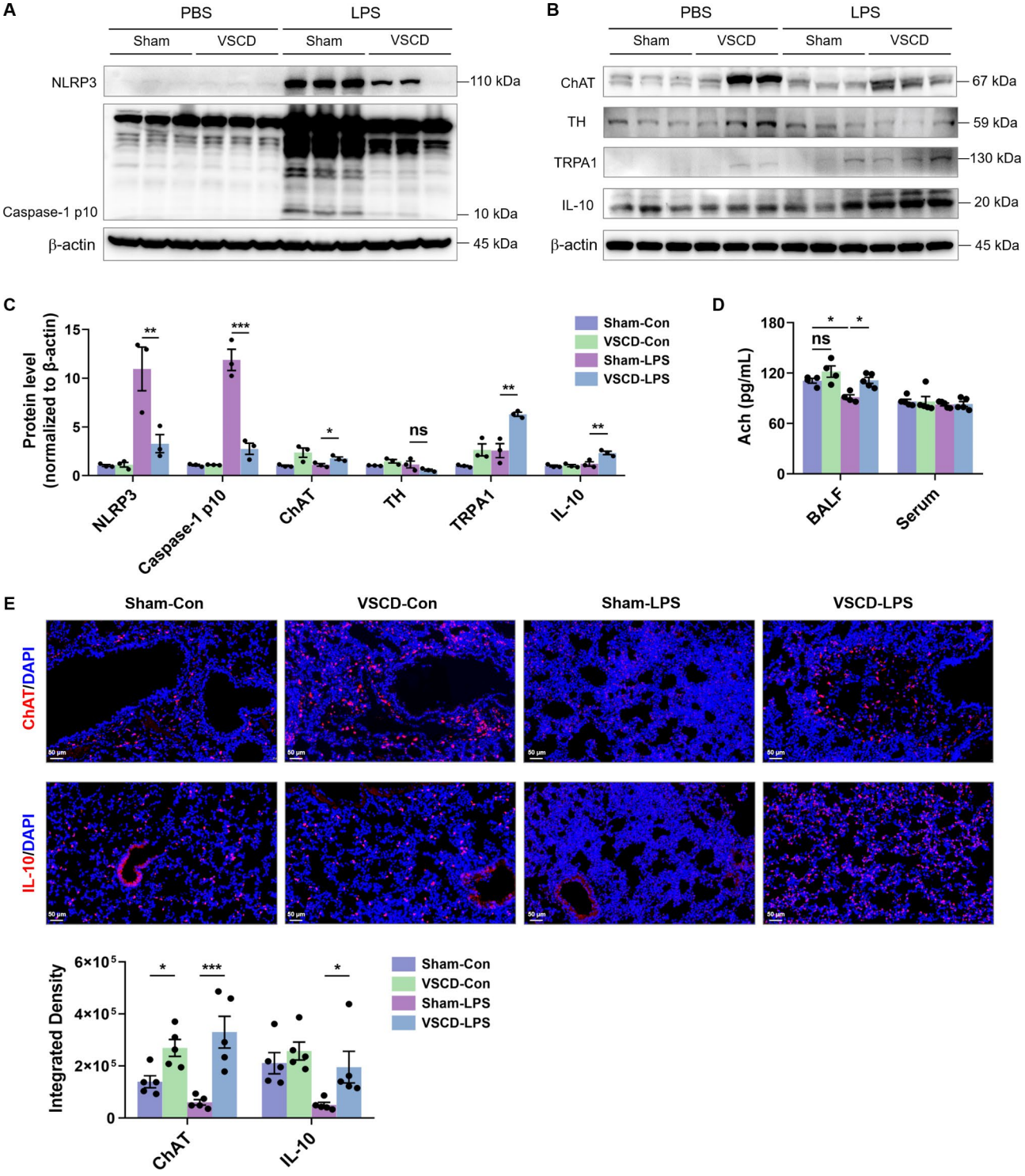

Fig. 6 VSCD (15s) dampens excessive inflammation and modulates parasympathetic innervation in lung tissues of ALI mice. **(A-C)** WB assay **(A, B)** and related quantitative assessments **(C)** demonstrating the regulatory effects of 15s-VSCD on NLRP3/Caspase-1 p10 expression for inflammasome activation, ChAT for parasympathetic innervation, TH for sympathetic innervation, TRPA1 for sensory innervation, and IL-10 expression for endogenous anti-inflammatory system. **(D)** VSCD elevated the production of Ach in the BALF, rather than serum of ALI mice. **(E)** Immunofluorescence staining and the quantitative analysis of ChAT and IL-10 (displayed in red) in lung sections from each group. Nuclei were stained with DAPI (4′, 6-Diamidino-2-phenylindole), shown in blue. Scale bar: 50 μm. $n = 3–5$ per group. $^{*}p < 0.05$, $^{**}p < 0.01$, $^{***}p < 0.001$, ns: not significant. Error bars represented mean ± SEM. Statistical analysis was performed using one-way ANOVA followed by Bonferroni's post hoc test

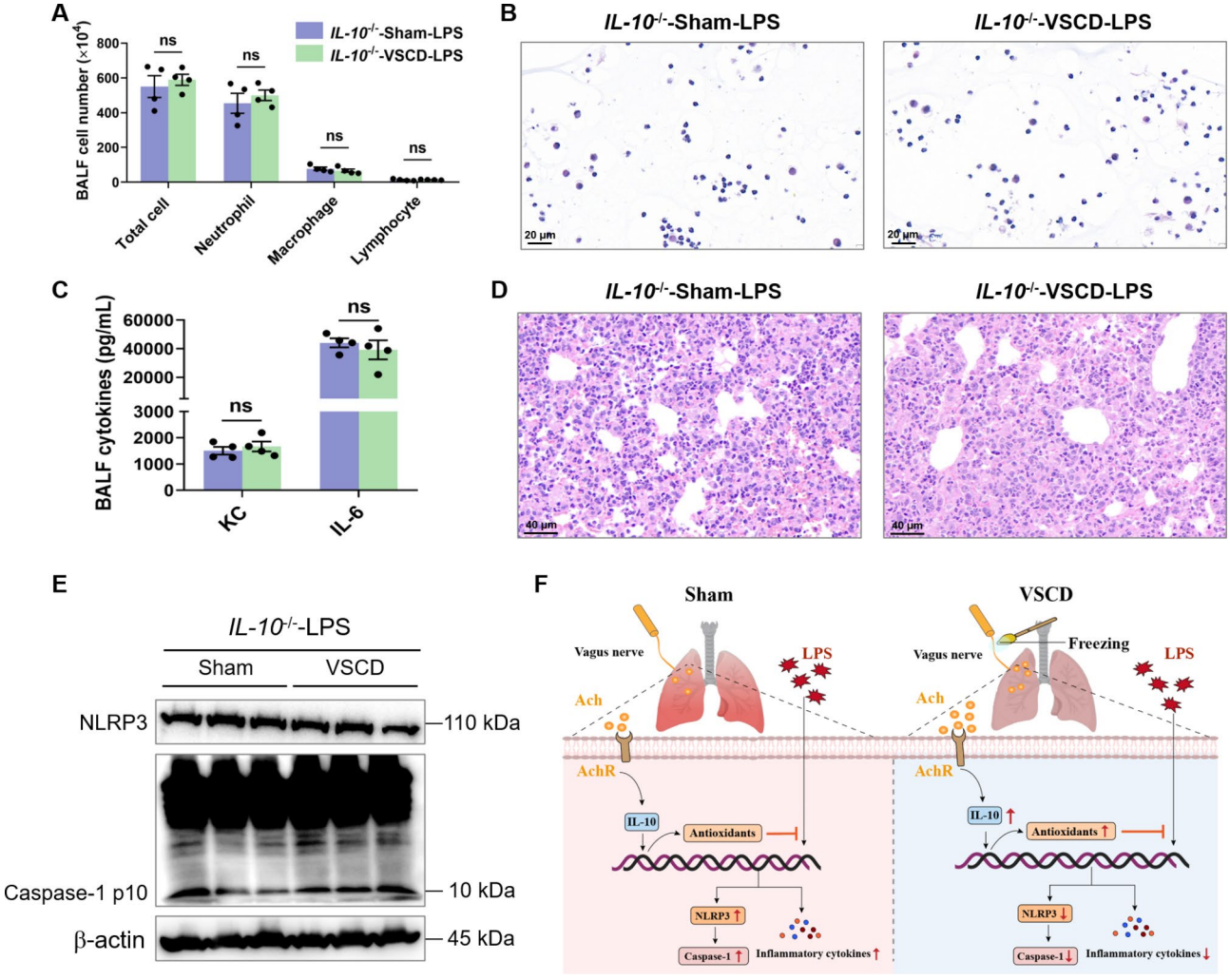

Fig. 7 IL-10 deficiency abolishes the protective property of VSCD in LPS-induced ALI model. **(A-C)** IL-10 knockout reversed VSCD-inhibited infiltration of inflammatory cells, especially neutrophils **(A, B)**, as well as the generation of cytokines KC, IL-6 **(C)** in the BALF of ALI mice. Scale bar: 20 μm. **(D)** Representative images of the lung sections stained with H&E from each group. Scale bar: 40 μm. **(E)** WB assay showing the critical role of IL-10 in the inhibitory action of VSCD on NLRP3/Caspase-1 p10 expression for lung inflammation. **(F)** Illustration summarizing the protective activity of VSCD in LPS-induced ALI mouse model. $n=4$ per group. ns: not significant. Error bars represented mean ± SEM. Statistical analysis was performed using two-tailed unpaired Student t test

survival of mice. Once proficient in the operation process and technical details, fatal bleeding in major blood vessels can be avoided and the overall survival of mice undergoing VSCD reaches nearly 100% (only 1 died from postoperative hypothermia).

VSCD causes morphological changes of mouse vagus nerve

To assess the effectiveness of VSCD procedure, mice were subjected to sham operation (Sham) or cryoablation by VSCD for 5/10/15s on the right cervical vagus nerve. At 1, 2, 3, and 4 weeks after surgery, nerve injury was examined from tissue histopathology. As shown in Fig. 2A **and B**, compared to the Sham group, effacement of the nerve architecture and vacuolar degeneration induced by VSCD were discovered since the first week after procedure, and the degree reached a peak at the second week. Besides, with the increase of freezing time, the extent of nerve injury gradually deepened. However, due to the existence of the self-repair mechanism, the restoration of vagus nerve damage has been found after 3 weeks post-surgery, with the changes of neuronal structure basically recovering at the fourth week (Fig. 2C **and D**). The findings elucidate the pathological morphological changes of vagus nerve within one month after VSCD.

In parallel to the H&E staining, we also stained nerve sections with protein gene product 9.5 (PGP9.5), a general neuronal marker expressed by neurons and nerve fibers. After VSCD operation, vagus nerve expressed lower level of PGP9.5 compared with the Sham group

since the first week (Fig. 3A). However, inconsistent with the results in Fig. 2, the immunostaining intensity of PGP9.5 kept decreasing by the end of the fourth week, indicating persistent damage to vagal innervation after VSCD (Fig. 3B-D). As one of the main organs innervated by the vagus nerve, the lungs from distinct groups were also collected and subjected to H&E staining. As shown in Figure S2, there was no obvious signs of injury or disturbances in the mouse lung following VSCD compared to the Sham group. Altogether, the results imply that cryodenervation by VSCD leads to a reliable and stable blockade of innervation, but reversible structural damage of mouse vagus nerve without detectable toxicity to lung tissues.

VSCD induces alterations in vagal innervation of the mouse lung

One of the main functions of vagus nerve is to protect organs like the lung. Accordingly, we investigated the impact of VSCD on pulmonary innervation, mainly including sensory nerve detected with TRPA1, parasympathetic nerve with ChAT, and sympathetic nerve with TH detection. Within two weeks after VSCD, the levels of TRPA1, ChAT, and TH in lung tissues elevated dramatically compared with the Sham mice, among which cryoablation for 15s exhibited the most significant effect (Fig. 4A, B **and E**). Shortly thereafter, the expression of these proteins began to decline, followed by falling below baseline (the Sham group) in the fourth week (Fig. 4C, D **and E**). By use of the immunofluorescence assay, we found that TRPA1, ChAT, and TH were distributed along the airways and blood vessels in mouse lung, which were consistent with previous studies [13, 17, 18]. Besides, the expression of the markers at the end of the first week after VSCD were basically consistent with the WB results (Figure S3). Based on these, both sensory and parasympathetic nerves in the mouse lung were significantly activated at the initial stage (1 week) after VSCD, and blocked three weeks later.

Since the cholinergic parasympathetic nerve controlling airway comes from the vagus nerve and exerts an anti-inflammatory effect by releasing Ach [19, 20], we estimated the role of VSCD in pulmonary immune microenvironment at one-week post-operation. As shown in Figure S4, VSCD downregulated pro-inflammatory NLRP3 activation, whereas elevated antioxidant HO-1 expression in lung tissues compared with the Sham group. Accordingly, we hypothesize that the short-term (1 week) effect of VSCD may be capable of alleviating excessive inflammation in pulmonary diseases and hold potential for clinical translation. To test this hypothesis, we investigated the efficacy of VSCD and related possible mechanisms by use of an LPS-induced mouse model of ALI/ARDS, also a classical model for acute pulmonary inflammation.

VSCD alleviates acute inflammation and lung damage in an ALI mouse model

To apply VSCD into ALI mouse model, LPS was instilled intranasally into mice to mimic the inflammatory microenvironment. The intervention group was subjected to 15s-VSCD or sham-operation randomly 1 week in advance, followed by detection 24 h later (Fig. 5A). First of all, VSCD did not cause additional airway inflammation nor lung tissue damage under physiological condition (Fig. 5C-E). Upon LPS challenge, the number of inflammatory cells, especially neutrophils in BALF were dramatically increased, which was partially reversed by VSCD procedure (Fig. 5B, C). To elucidate local and systemic inflammation of mice, we next detected the secretion of neutrophil chemokine KC and pro-inflammatory cytokine IL-6 both in BALF and serum. Rather than sham-operation, VSCD decreased KC and IL-6 levels in the airway and serum of ALI mice (Fig. 5D). Furthermore, the severity of lung injury in mice from each group was evaluated via pathological tissue slides according to five histopathological features: alveolar and interstitial neutrophils, hyaline membranes formation, proteinaceous debris within airspaces, and alveolar septal thickening. It could be observed that VSCD alleviated pulmonary damage induced by LPS compared to the Sham group (Fig. 5E).

To comprehensively verify the protective effect of VSCD against LPS-induced lung inflammation, we prepared tissue homogenate and extracted proteins for immunoblotting assay. Consistent with the findings above, VSCD was found to suppress the over-activation of NLRP3/Caspase-1 pro-inflammatory pathway in ALI mouse lung (Fig. 6A, C). Meanwhile, VSCD upregulated the expression of IL-10, which is a canonical immunosuppressive factor with potent anti-inflammatory property in multiple diseases [21](Fig. 6B, C). This suggested an enhanced endogenous resistance caused by VSCD to LPS-induced lung injury. Considering the altered vagal innervation in the airways upon VSCD, we then measured the expression of functional neural markers ChAT, TH, and TRPA1 in the lungs of ALI mouse model. As shown in Fig. 6B, C, levels of cholinergic neuronal marker ChAT and sensory neuronal marker TRPA1, rather than sympathetic neuronal marker TH, were significantly elevated by VSCD under LPS stimulation. Furthermore, VSCD also increased the production of anti-inflammatory neurotransmitter Ach in BALF, but not in serum of ALI mice (Fig. 6D). Consistently, we observed similar change trends of ChAT and IL-10 expression in mouse lung using immunofluorescence technique (Fig. 6E). Accordingly, the results indicate that an activated

cholinergic anti-inflammatory pathway (CAP) in the lung may explain the protective action of VSCD following LPS challenge.

IL-10 deficiency partially abrogated the protective action of VSCD in the ALI mouse model

Based on the above results (Fig. 6B, C) and the previous literature [22, 23], we speculated that VSCD/CAP-elevated IL-10 expression might trigger the anti-inflammatory effect under LPS challenge. To confirm this, we applied *IL-10*$^{-/-}$ mice to construct the ALI model with or without VSCD surgery. Contrary to the findings in WT mice (Fig. 5), VSCD could not inhibit the accumulation of total inflammatory cells, including neutrophils, as well as the secretion of KC, IL-6 in the BALF of ALI mice with IL-10 deficiency (Fig. 7A-C). Meanwhile, it was clearly observed that IL-10 depletion abolished the protective action of VSCD in LPS-induced tissue damage (Fig. 7D). Besides, IL-10 knockout also reversed the decreased activation of inflammatory NLRP3/Caspase-1 pathway by VSCD in lung tissues of ALI mouse model (Fig. 7E). Collectively, the data verify that VSCD activate CAP, which exerts anti-inflammatory and protective effects in the lung of ALI mice probably through an upregulation of IL-10 expression (Fig. 7F).

Discussion

The involvement of neuroimmune crosstalk in the initiation and progression of lung inflammation has been increasingly recognized [20]. Activated immune cells release cytokines that bind to receptors on nearby endings of peripheral afferent nerves, relaying inflammatory signals to the brain. These signals are then transmitted through efferent nerves, which secrete neurotransmitters that act on immune cells to modulate the pulmonary inflammatory responses [24]. Therefore, targeting neuroimmune pathways may offer a novel therapeutic approach for associated disorders. Compared to pharmacological options, researchers aim to achieve long-term or permanent relief from symptoms of several lung diseases through interventional techniques [25, 26]. Bronchial thermoplasty (BT), for instance, is a non-pharmacological treatment for severe asthma, heating the airway wall to reduce smooth muscle and alleviate asthma symptoms [27]. Nevertheless, the precise mechanism behind this technique remains unclear. Some researchers speculate that the additional nerve-ablating action of BT also contributes to its efficacy in improving severe asthma [28]. If the therapeutic benefit of BT via denervation is incidental, then TLD is explicitly designed to disrupt parasympathetic innervation for COPD treatment [25]. Recently, we develop a novel cryo-balloon TLD system, abbreviated as BCD, in the management of severe asthma. Unlike BT or traditional TLD procedure, BCD requires only up to four freeze-thaw cycles to achieve circumferential denervation of the main bronchi, with each cycle lasting no more than five minutes. This means the entire procedure can be completed during a single bronchoscopic session, and indicates a major breakthrough for the interventional therapy of severe asthma [12].

The aforementioned attempts represent clinical endeavors for airway inflammatory diseases via neuroimmune signaling pathway. However, the underlying mechanism has yet to be fully validated, particularly within the context of commonly employed rodent models. Up to now, resection and anesthesia are the two methods for vagus nerve blockage in mouse, significantly differing from those used in clinical practice [13, 29]. Therefore, we introduce a novel cryodenervation technique, abbreviated as VSCD, to mimic the clinical situation and investigate the mechanism in the mouse model (Fig. 1, Movie S1). Our surprise is occasioned by the VSCD, which is intended to ablate nerve function, instead leads to enhanced lung innervation by three major nerves one week post the surgery (Fig. 4). As the process of neural reinnervation takes at least three months [30], we speculate this effect may be due to a reflex response triggered by sensory nerves within the vagus nerve in response to direct cryodamage rather than reinnervation after injury. Conversely, parasympathetic and sympathetic nerves can't directly perceive external stimuli due to the lack of nociceptors. The activation of these nerves thus originates from sensory neural signals processed by central nervous system [31]. Besides, the balance between parasympathetic and sympathetic nerve systems may also play a role in this process, as occurs in heart diseases [32]. Moreover, the elevated lung innervations observed at the first week post-VSCD raise previously unconsidered questions: what is the impact of increased neural excitability on patients with asthma during early stage after operation; how should this be addressed in clinical trials? These problems are also pertinent to BT and traditional TLD operation, and need to be further concerned in future research.

An important issue that affects denervation is the intrinsic self-repair capacity of peripheral nerves following damage. Cellular swelling is usually the earliest change observed in cryodamage, and in severe case, vacuolar degeneration occurs. Specifically, rapid cooling results in the formation of intracellular ice crystals, which can impair the plasma membrane. When frozen cells thaw, the ice in the extracellular space melts, making it hypotonic compared to the intracellular compartment. As a consequence, there may be a transfer of osmotic fluid, inducing vacuolar degeneration of the cells [33, 34]. In addition, cryoablation also causes indirect injury to cells via thrombus formation in post-thaw period [35]. Upon recovery, increased temperature restores

integrity and fluidity of the membrane, and the activity of certain membrane proteins such as ion channels and transporters. This allows reestablishment of normal ionic concentration gradients and osmotic balance, thus expelling excess water from the cell and reducing swelling of cytoplasmic organelles. Afterwards, the functional restoration of mitochondria, lysosomes, and endoplasmic reticulum can elevate cellular energy metabolism, eliminate excess or damaged substances, and accelerate protein and lipid synthesis, contributing to the disappearance of vacuolization [36]. In the present study, we ablate mouse vagus nerve with liquid nitrogen pen, with the epineurium largely intact after VSCD. Additionally, we report, for the first time, the self-repair process of mouse vagus nerve following cryoablation on a weekly basis (Figs. 2 and 3). By the fourth week post-operation, vacuolar degeneration caused by VSCD has been significantly improved, indicating the neuromorphological repair of the vagus nerve that may be related to the above mechanisms. However, vagal innervation of target organs, indicated by PGP9.5 presented in neurons and nerve fibers, is still declining at that time. Meanwhile, pulmonary markers of sensory and parasympathetic innervation are also reduced four weeks after VSCD surgery (Fig. 4). We thus consider that the recovery time of nerve innervation is longer than that of morphological appearance. This discrepancy can be explained. Even reversible injury can cause various functional impairments in neurons, and the degree of this impact depends on the number and repair ability of these cells [36]. With the morphological restoration of vagus nerve, the function of sensory and parasympathetic nerves is very likely to return after a long time [14], perhaps months to years in the case of 15s-VSCD. It still remains unknown whether vagal innervation could be restored to normal level after VSCD; and when will it be returned. Given that neural repair has a great impact on the application of VSCD in chronic respiratory diseases, represented by asthma and COPD, long-term observation of vagus nerve function and its control over the lung is necessary and will be included in our future study.

Herein, we discover that three major nerves innervating the lung were activated at the early phase (1 week) following VSCD, accompanied by inhibition of the NLRP3 inflammasome and activation of HO-1 antioxidant pathway in mouse lung under physiological condition (Fig. 4, Figure S3-4). Therefore, we speculate that activated CAP plays a dominant role during the early stage of VSCD mouse model and employ an ALI model to validate its effectiveness. As shown in Fig. 5, VSCD exhibits an anti-inflammatory effect against LPS-induced acute lung inflammation via restraining chemokine/cytokine production, thereby reducing pulmonary damage. As key indicator or effector of the CAP, ChAT expression in lung tissues and Ach secretion in BALF are also elevated by VSCD in ALI mice compared with the Sham group (Fig. 6). The findings are consistent with previous studies demonstrating that CAP activation by either direct stimulation or pharmaceuticals could diminish excessive inflammatory responses in multiple diseases [20, 37–39]. Mechanistically, we suppose that VSCD-activated CAP dampens excess inflammation and lung injury through an increased expression of potent anti-inflammatory IL-10. In accordance with other study showing that Ach promoted IL-10 secretion via binding to nicotinic Ach receptor [23], we similarly identify an enhanced IL-10 generation in ALI mouse lung after VSCD along with the upregulation of ChAT and Ach. Moreover, we apply IL-10 knockout mouse into the ALI model to further investigate the role of IL-10 in the protective effect of VSCD. As exhibited in Fig. 7, IL-10 deficiency abrogates the therapeutic action of VSCD in LPS-triggered ALI mice, including excessive leukocytes aggregation, pro-inflammatory cytokine secretion, and NLRP3 inflammasome activation. These lines of evidence suggest that VSCD acting through CAP/IL-10 can exert anti-inflammatory effect in mouse lung following LPS exposure. It should be noted that although researcher have applied vagus nerve stimulation as prophylactic strategy for LPS-induced tissue injuries [40], the optimal use time of VSCD still needs to be precisely explored in order to adapt to clinical demand.

Although this research is a pioneering effort to fill the gap in mouse vagus nerve cryoablation, it does have some limitations. Firstly, the vagal innervation of mouse lung with VSCD is determined by measuring protein level of specific neural markers; however, direct visualization of the innervation could be done via CRISPR-CAS9 gene editing technology. Additionally, the morphology and innervation of vagus nerve after VSCD should be monitored for a longer period of time (at least six months). Considering the important role of neuroimmune cross-talk in the efficacy of VSCD, further study is needed on discovering the target cell types in the lung and investigating the anti-inflammatory mechanisms of VSCD on these cells, thus guiding the application of BCD in clinical management of several pulmonary diseases, such as asthma and COPD.

Conclusion

In the present study, we develop a practical method for mouse peripheral nerve cryoablation (VSCD). VSCD is demonstrated to be feasible and safe for mouse vagal denervation. It also induces a reliable and stable blockade of innervation, but reversible structural damage of mouse vagus nerve without detectable toxicity to lung tissues. Interestingly, cholinergic parasympathetic nerve in the mouse lung coming from vagus nerve is activated at the

initial stage after VSCD, and blocked three weeks later. The short-term effect (1 week) of VSCD is then evaluated on an ALI mouse model. The data showed that VSCD effectively decreased pulmonary inflammation and tissue damage in the ALI mice. Mechanistically, the activated CAP and elevated IL-10 expression may explain the protective action of VSCD upon LPS challenge. This study not only fills the gap in mouse vagus nerve cryoablation, thereby guiding the application of cryodenervation in clinical management of asthma and COPD, but also opens novel therapeutic avenues for the intervention of acute lung inflammation.

Abbreviations

VSCD	Visualized and simple cryodenervation
ALI	Acute lung injury
LPS	Lipopolysaccharide
CAP	Cholinergic anti-inflammatory pathway
TLD	Targeted lung denervation
COPD	Chronic obstructive pulmonary disease
BCD	Bronchial cryodenervation
IL-10	Interleukin-10
H&E	Haematoxylin-eosin
BALF	Bronchoalveolar lavage fluid
KC	Keratinocyte-derived chemokine
Ach	Acetylcholine
TRPA1	Transient receptor potential ankyrin 1
ChAT	Choline acetyltransferase
TH	Tyrosine hydroxylase
TBST	Tris-buffered saline containing 0.1% Tween 20
SEM	Standard error
Sham	Sham operation
PGP9.5	Protein gene product 9.5
BT	Bronchial thermoplasty

Supplementary Information

The online version contains supplementary material available at https://doi.org/10.1186/s12931-025-03108-w.

Supplementary Material 1

Supplementary Material 2

Supplementary Material 3

Acknowledgements
We thank BioRender for providing fundamental materials of our scheme figure (Fig. 5A).

Author contributions
W.G., Q.L. and D.W. conceived and designed the study, and are responsible for this manuscript. D.W., X.L., J.G., and K.W. carried out the experiments with technical guidance from W.G., W.X. and F.W. D.W., X.L. and Z.J. coordinated to analyze experimental data and write the draft. W.G., Q.L. and D.W. revised the article in detail. All authors read and approved the final manuscript.

Funding statement
This work was supported by National Natural Science Foundation of China (grant number: 82000086), Pudong New Area Health Commission Health Talent Training Project Plan (grant number: 2025PDWSYCQN-02) for Wei Gao; The Top-level Clinical Discipline Project of Shanghai Pudong (grant number: PWYgf2021-05), National Natural Science Foundation of China (grant number: 82070086, 82270116), Yunnan Li Qiang Expert Workstation (grant number: 202305AF150137) for Qiang Li; Nantong Health Commission Scientific Research Projects (grant number: QN2022018) for Dandan Wu; and National Natural Science Foundation of China (grant number: 82160593), Yunnan Applied Basic Research Projects (grant number: 202201AY070001-197, 202101AY070001-213) for Zhixian Jin.

Data availability
No datasets were generated or analysed during the current study.

Declarations

Ethics approval and consent to participate
All experiments performed on animals were in accordance with the guide for Care and Use of Laboratory Animals from Shanghai Committee. Meanwhile, the research protocol has been recognized by Laboratory Animal Research Center Review Board of Tongji University (Permit Number: TJBB03721106) (Shanghai, China). All operations were conducted under pentobarbital sodium anesthesia, and every effort was made to minimize animal suffering and the number of animals used.

Consent for publication
Not Applicable.

Competing interests
The authors declare no competing interests.

Clinical trial number
Not Applicable.

Author details
[1]Department of Pulmonary and Critical Care Medicine, Shanghai East Hospital, School of Medicine, Tongji University, Shanghai 200092, China
[2]Department of Pulmonary and Critical Care Medicine, Affiliated Calmette Hospital of Kunming Medical University and The First People's Hospital of Kunming City, Yunnan 650224, China
[3]Department of Respiratory and Critical Care Medicine, The Second Affiliated Hospital of Nantong University, Nantong 226001, China

Received: 27 September 2024 / Accepted: 8 January 2025
Published online: 13 January 2025

References

1. Nikolai NK. A history of cryosurgery: its development and future. J Am Coll Surg 2007, 204.
2. Kwak K, Yu B, Lewandowski RJ, Kim DH. Recent progress in cryoablation cancer therapy and nanoparticles mediated cryoablation. Theranostics. 2022;12:2175–204.
3. Yakkala C, Denys A, Kandalaft L, Duran R. Cryoablation and immunotherapy of cancer. Curr Opin Biotechnol. 2020;65:60–4.
4. Fintelmann FJ, Braun P, Mirzan SH, Huang AJ, Best TD, Keyes CM, Choy E, Leppelmann KS, Muniappan A, Soto DE, et al. Percutaneous Cryoablation: Safety and Efficacy for Pain Palliation of metastases to Pleura and Chest Wall. J Vasc Interv Radiol. 2020;31:294–300.
5. Yoon JH, Grechushkin V, Chaudhry A, Bhattacharji P, Durkin B, Moore W. Cryoneurolysis in patients with refractory chronic Peripheral Neuropathic Pain. J Vasc Interv Radiol. 2016;27:239–43.
6. Andrade J, Wells G, Deyell M, Bennett M, Essebag V, Champagne J, Roux J, Yung D, Skanes A, Khaykin Y, et al. Cryoablation or Drug Therapy for initial treatment of Atrial Fibrillation. N Engl J Med. 2021;384:305–15.
7. Zhao ZR, Lau RWH, Ng CSH. Catheter-based alternative treatment for early-stage lung cancer with a high-risk for morbidity. J Thorac Dis. 2018;10:S1864–70.
8. Velez A, DeMaio A, Sterman D. Cryoablation and immunity in non-small cell lung cancer: a new era of cryo-immunotherapy. Front Immunol. 2023;14:1203539.
9. Pison C, Shah PL, Slebos DJ, Ninane V, Janssens W, Perez T, Kessler R, Deslee G, Garner JL, Hartman JE, et al. Safety of denervation following targeted lung denervation therapy for COPD: AIRFLOW-1 3-year outcomes. Respir Res. 2021;22:62.
10. Shawn DA, Donald AM. Calming Nervous airways: targeted Lung Denervation for Chronic Obstructive Pulmonary Disease. Am J Respir Crit Care Med 2019, 200.

11. Wang K, Sun J, Gao W, Chen R, Wu X, He Y, Guo Q, Zhang X, Li Q. Feasibility, effectiveness, and safety of a novel cryo-balloon targeted lung denervation technique in an animal model. Cryobiology. 2020;93:27–32.
12. Wang K, Gao S, Sun J, Liao X, Zhang X, Chen R, Tang R, Wang Y, Shang Y, Xu W, Li Q. Bronchial cryo-denervation for severe asthma: a pilot study. Respiration. 2024;103:155–65.
13. Zhang X, Wei X, Deng Y, Yuan X, Shi J, Huang W, Huang J, Chen X, Zheng S, Chen J, et al. Mesenchymal stromal cells alleviate acute respiratory distress syndrome through the cholinergic anti-inflammatory pathway. Signal Transduct Target Ther. 2022;7:307.
14. Gage AA, Baust JM, Baust JG. Experimental cryosurgery investigations in vivo. Cryobiology. 2009;59:229–43.
15. Boulan B, Beghin A, Ravanello C, Deloulme JC, Gory-Fauré S, Andrieux A, Brocard J, Denarier E. AutoNeuriteJ: an ImageJ plugin for measurement and classification of neuritic extensions. PLoS ONE. 2020;15:e0234529.
16. Matute-Bello G, Downey G, Moore BB, Groshong SD, Matthay MA, Slutsky AS, Kuebler WM. An official American Thoracic Society workshop report: features and measurements of experimental acute lung injury in animals. Am J Respir Cell Mol Biol. 2011;44:725–38.
17. Su Y, Barr J, Jaquish A, Xu J, Verheyden JM, Sun X. Identification of lung innervating sensory neurons and their target specificity. Am J Physiol Lung Cell Mol Physiol. 2022;322:L50–63.
18. Wang W, Cohen JA, Wallrapp A, Trieu KG, Barrios J, Shao F, Krishnamoorthy N, Kuchroo VK, Jones MR, Fine A, et al. Age-related dopaminergic innervation augments T helper 2-Type allergic inflammation in the postnatal lung. Immunity. 2019;51:1102–e11181107.
19. Vida G, Peña G, Deitch EA, Ulloa L. α7-cholinergic receptor mediates vagal induction of splenic norepinephrine. J Immunol. 2011;186:4340–6.
20. Wu D, Liao X, Gao J, Gao Y, Li Q, Gao W. Potential pharmaceuticals targeting neuroimmune interactions in treating acute lung injury. Clin Transl Med. 2024;14:e1808.
21. Ouyang W, O'Garra A. IL-10 family cytokines IL-10 and IL-22: from Basic Science to Clinical Translation. Immunity. 2019;50:871–91.
22. Wang K, Wang M, Liao X, Gao S, Hua J, Wu X, Guo Q, Xu W, Sun J, He Y, et al. Locally organised and activated Fth1(hi) neutrophils aggravate inflammation of acute lung injury in an IL-10-dependent manner. Nat Commun. 2022;13:7703.
23. Zheng W, Song H, Luo Z, Wu H, Chen L, Wang Y, Cui H, Zhang Y, Wang B, Li W et al. Acetylcholine ameliorates colitis by promoting IL-10 secretion of monocytic myeloid-derived suppressor cells through the nAChR/ERK pathway. Proc Natl Acad Sci U S A 2021, 118.
24. Azzoni R, Perdijk O, Harris N, Marsland B. Neuroimmune Interactions in the Lung. *Annual review of immunology* 2023.
25. Aaron SD, Mahler DA. Calming Nervous airways: targeted Lung Denervation for Chronic Obstructive Pulmonary Disease. Am J Respir Crit Care Med. 2019;200:1455–6.
26. Liao X, Gao S, Xie F, Wang K, Wu X, Wu Y, Gao W, Wang M, Sun J, Liu D, et al. An underlying mechanism behind interventional pulmonology techniques for refractory asthma treatment: Neuro-immunity crosstalk. Heliyon. 2023;9:e20797.
27. Russell RJ, Brightling CE. Bronchial thermoplasty: what we know, what we don't know, and what we need to know. Eur Respir J 2022, 59.
28. Facciolongo N, Di Stefano A, Pietrini V, Galeone C, Bellanova F, Menzella F, Scichilone N, Piro R, Bajocchi GL, Balbi B, et al. Nerve ablation after bronchial thermoplasty and sustained improvement in severe asthma. BMC Pulm Med. 2018;18:29.
29. Jin H, Li M, Jeong E, Castro-Martinez F, Zuker CS. A body-brain circuit that regulates body inflammatory responses. Nature. 2024;630:695–703.
30. Bregeon F, Alliez JR, Héry G, Marqueste T, Ravailhe S, Jammes Y. Motor and sensory re-innervation of the lung and heart after re-anastomosis of the cervical vagus nerve in rats. J Physiol. 2007;581:1333–40.
31. Mazzone SB, Undem BJ. Vagal Afferent Innervation of the Airways in Health and Disease. Physiol Rev. 2016;96:975–1024.
32. Khan AA, Lip GYH, Shantsila A. Heart rate variability in atrial fibrillation: the balance between sympathetic and parasympathetic nervous system. Eur J Clin Invest. 2019;49:e13174.
33. Baust JG, Gage AA. The molecular basis of cryosurgery. BJU Int. 2005;95:1187–91.
34. Erinjeri JP, Clark TW. Cryoablation: mechanism of action and devices. J Vasc Interv Radiol. 2010;21:S187–191.
35. S M W FT Jr, D O C L, T W, S G C. D M M: Perivascular and intralesional tissue necrosis after hepatic cryoablation: results in a porcine model. Surgery 1997, 122.
36. Miller MA, Zachary JF. Mechanisms and morphology of cellular injury, adaptation, and death. Pathologic Basis Veterinary Disease 2017:2.
37. Zhao M, He X, Bi XY, Yu XJ, Gil Wier W, Zang WJ. Vagal stimulation triggers peripheral vascular protection through the cholinergic anti-inflammatory pathway in a rat model of myocardial ischemia/reperfusion. Basic Res Cardiol. 2013;108:345.
38. Borovikova LV, Ivanova S, Zhang M, Yang H, Botchkina GI, Watkins LR, Wang H, Abumrad N, Eaton JW, Tracey KJ. Vagus nerve stimulation attenuates the systemic inflammatory response to endotoxin. Nature. 2000;405:458–62.
39. van Maanen MA, Vervoordeldonk MJ, Tak PP. The cholinergic anti-inflammatory pathway: towards innovative treatment of rheumatoid arthritis. Nat Rev Rheumatol. 2009;5:229–32.
40. Go YY, Ju WM, Lee CM, Chae SW, Song JJ. Different Transcutaneous Auricular Vagus nerve stimulation parameters modulate the anti-inflammatory effects on Lipopolysaccharide-Induced Acute inflammation in mice. Biomedicines 2022, 10.

Publisher's note